Journal of Solid State Chemistry 182 (2009) 2219–2224

Contents lists available at ScienceDirect

Journal of Solid State Chemistry

journal homepage: www.elsevier.com/locate/jssc

Visible quantum cutting through downconversion in $GdPO_4:Tb^{3+}$ and $Sr_3Gd(PO_4)_3:Tb^{3+}$

Deyin Wang [a,b], Nobuhiro Kodama [b,*]

[a] School of Physical Science and Technology, Key Laboratory for Magnetism and Magnetic Materials of the Ministry of Education, Lanzhou University, Lanzhou 730000, PR China
[b] Department of Materials Science and Engineering, Faculty of Engineering and Resource Science, Akita University, Akita 010-8502, Japan

ARTICLE INFO

Article history:
Received 15 January 2009
Received in revised form
12 May 2009
Accepted 17 May 2009
Available online 30 May 2009

Keywords:
Quantum cutting
Downconversion

ABSTRACT

Visible quantum cutting has been observed in $GdPO_4:Tb^{3+}$ upon Tb^{3+} $4f^8$–$4f^75d^1$ excitation and host excitation, and in $Sr_3Gd(PO_4)_3:Tb^{3+}$ upon Tb^{3+} $4f^8$–$4f^75d^1$ excitation. In the quantum cutting process, Tb^{3+} acts as a quantum cutter, which converts one short wavelength ultraviolet photon or one vacuum ultraviolet photon into more than one visible photon. The quantum cutting involves a cross-relaxation process between two neighboring Tb^{3+} and direct energy transfer between Tb^{3+} and Tb^{3+} or Tb^{3+} and Gd^{3+}, depending on the excitation wavelength. The quantum efficiency variation of $GdPO_4:xTb^{3+}$ and $Sr_3Gd(PO_4)_3:xTb^{3+}$ shows a growing trend with increasing of Tb^{3+} content from $x = 1.5\%$ to 13%.

1. Introduction

Quantum cutting of rare-earth doped phosphors in the vacuum ultraviolet (VUV) region has gained increasing attention recently as a method for enhancing the conversion efficiency of phosphors used in Hg-free fluorescent lamps and color plasma display panels, in which VUV radiation from noble gas discharge is used as the excitation source. Quantum cutting is a phenomenon that occurs in materials that emit more than one photon per photon absorbed [1]. It is possible in theory, because a VUV photon has more than twice the energy of a visible photon. Quantum cutting can be realized via two different mechanisms [2]: photon cascade emission and cross relaxation energy transfer (CRET); the process involved in CRET is also known as downconversion [3,4]. Photon cascade emission was generated by using emission from Pr^{3+} and Gd^{3+} in phosphors [5–10]. In these phosphors, however, the first photon for Pr^{3+} has a wavelength of 406 nm [5–8] and the second photon for Gd^{3+} has a wavelength of 311 nm [9,10]; these emissions are too short for lighting and display application. Quantum cutting via CRET has been mainly investigated in fluoride [1,3,4,11–17] using appropriate combinations of $R_1^{3+}-R_2^{3+}$ and $R_1^{3+}-R_2^{3+}-R_3^{3+}$ ($R_1 = Gd$, $R_2 = Eu$ and Tb and $R_3 = Er$). In particular, a quantum cutting efficiency closed to 200% has been achieved in $LiGdF_4:Eu^{3+}$ [1] and $BaF_2:Gd^{3+}$, Eu^{3+} [16]. Although fluorides with wide band gap are still the best candidates for investigating quantum cutting, they are very sensitive to oxygen surface contamination, which may influence their luminescence properties and limit their application. Compared with fluorides, oxide phosphors are more chemically stable and easier to prepare. If the band gap of an oxide is large enough, the $4f5d$ or $4f$ state of rare earth ions will be located within the host band gap, making it possible to realize quantum cutting in such an oxide.

$GdPO_4$ and $Sr_3Gd(PO_4)_3$ have been reported to have a host related absorption with maximum around 155 [18–22] and 170 nm [23], respectively. This satisfies the requirement for a QC phosphor to be transparent in the VUV region. Several studies have discussed the energy transfer between Gd^{3+} and Tb^{3+} in $GdPO_4$ [21,22], and concluded that Gd^{3+} transferred the excitation energy from its ^6P_J level to a neighboring Tb^{3+}. However, there is little consideration regarding the quantum cutting between Tb^{3+}–Tb^{3+} in $GdPO_4$ or $Sr_3Gd(PO_4)_3$. In a sense, quantum cutting can be considered to be a new concept for explaining the energy transfer process. In this study, $GdPO_4:Tb^{3+}$ and $Sr_3Gd(PO_4)_3:Tb^{3+}$ are investigated based on the quantum cutting model proposed for $K_2GdF_5:Tb^{3+}$ [3] and $BaGdF_5:Tb^{3+}$ [4] in an effort to verify the possibility of quantum cutting in oxides and to explain the energy transfer mechanism in them.

2. Experimental

$GdPO_4:xTb^{3+}$ (1.5%, 3%, 5%, 7%, 9%, 11% and 13%) and $Sr_3Gd(PO_4)_3:xTb^{3+}$($x = 1.5\%$, 3%, 5%, 7%, 11% and 13%) were synthesized by solid state reactions. Gd_2O_3 (4N), Tb_4O_7 (4N), $(NH_4)_2HPO_4$ (4N) and $SrCO_3$ (4N) were used as the raw materials. The corresponding raw materials were weighed in stoichiometric ratios, grounded, pressed and then fired at different conditions.

* Corresponding author. Fax: +81 18 8892601.
E-mail address: kodama@ipc.akita-u.ac.jp (N. Kodama).

0022-4596/$ - see front matter © 2009 Elsevier Inc. All rights reserved.
doi:10.1016/j.jssc.2009.05.026

$GdPO_4$:xTb^{3+} was firstly fired at 1150 °C for 6 h, then fired at 850 °C for 5 h in a reducing atmosphere of 5% H_2–95% Ar; $Sr_3Gd(PO_4)_3$:xTb^{3+} was fired firstly at 600 °C for 4 h and then at 1250 °C for 4 h. All samples obtained were white in color.

The phase purity of all the samples was verified by powder X-ray diffraction (XRD; a Rigaku, Rint 2000 V). The VUV excitation and emission spectra were measured at room temperature by a fluorescence spectrophotometer (Kokenkogyo, VUV-2000) equipped with a deuterium lamp as the lighting source. The UV and visible emission were dispersed by the spectrophotometer and were detected by a photomultiplier tube. Excitation spectra were obtained by scanning the VUV monochromator that had VUV coated gratings blazed at 150 nm. The VUV excitation spectra were corrected by using sodium salicylate as a standard. The spectral resolution of this instrument for emission and excitation was approximately 1 and 2 nm, respectively.

3. Results and discussion

3.1. XRD of $GdPO_4$:xTb^{3+} and $Sr_3Gd(PO_4)_3$:xTb^{3+}

$GdPO_4$ crystallizes in a monoclinic monazite structure with space group $P2_1/n$, and the Gd atoms in this structure are nine-coordinated with a C_S symmetry [24]. $Sr_3Gd(PO_4)_3$ has a eulytite structure with space group $I\bar{4}3d$, and Sr and Gd occupy the same site with a C_3 symmetry [23,25]. Fig. 1 shows the XRD patterns of $GdPO_4$:xTb^{3+} ($1.5\% \le x \le 13\%$) and $Sr_3Gd(PO_4)_3$:xTb^{3+}($1.5\% \le x \le 13\%$). All diffraction peaks of $GdPO_4$:xTb^{3+} are in good agreement with JCPDS card No. 32–0386. With the exception of the two small peaks ($I\% < 3\%$) indicated by an asterisk, which could not be identified, the rest of diffraction peaks of $Sr_3Gd(PO_4)_3$:xTb^{3+} could be well indexed according to JCPDS card No. 29–1301.

3.2. Photoluminescence properties of $GdPO_4$:xTb^{3+}

Fig. 2 presents the excitation spectra of $GdPO_4$:xTb^{3+} ($1.5\% \le x \le 13\%$) in the range of 120 to 300 nm. All the excitation spectra are the same except for their intensities. The spectra consist of three bands. The first band located in the range 140–165 nm is ascribed to the host band absorption, which is probably in connection with the intramolecular transition of the PO_4^{3-} group [18–21]. The second broad band in the range 165–225 nm is assigned to the intraconfiguration $4f^8$–$4f^7 5d^1$ transition of Tb^{3+} [18–22]. The third band with a peak at 273 nm is attributed to the $^8S_{7/2}$–^6I_J transition of Gd^{3+} ions. When one electron of Tb^{3+} is promoted from the ground states $4f^8$ to the $4f^7 5d^1$ excited state, it can produce two kinds of $4f^8$–$4f^7 5d^1$ transitions: spin-allowed and spin-forbidden transitions. The spin-allowed transition is more energetic than the spin-forbidden transitions [22]. Due to the low symmetry of the Tb^{3+} site in $GdPO_4$:xTb^{3+} [26], the broad $4f^8$–$4f^7 5d^1$ transition band is split into several small bands, and the small bands with peaks at 168, 180, 196 and 204 nm are considered to originate from the spin-allowed $4f^8$–$4f^7 5d^1$ transition of Tb^{3+}. The shoulder of the broad band at 221 nm was assigned to the spin-forbidden $4f^8$–$4f^7 5d^1$ transition of Tb^{3+}, which had been evaluated by using the position of the 4*f*–5*d* band of Ce^{3+} in $GdPO_4$ [18]. Even the shoulder was calculated to be due to the spin-forbidden $4f^8$–$4f^7 5d^1$ transition of Tb^{3+}, we consider that the splitting of the 5*d* orbit also contributes to the origin of the shoulder. In addition, the small band with a peak at 196 nm has nearly the same position as the ^6G_J–$^8S_{7/2}$ transition of Gd^{3+} observed in some fluorides [1,11–15]. In view of the ^6G_J–$^8S_{7/2}$ transition of Gd^{3+} is spin and parity forbidden, it is thought that the peak at 196 nm mainly originates from splitting of the 5*d* band of Tb^{3+}.

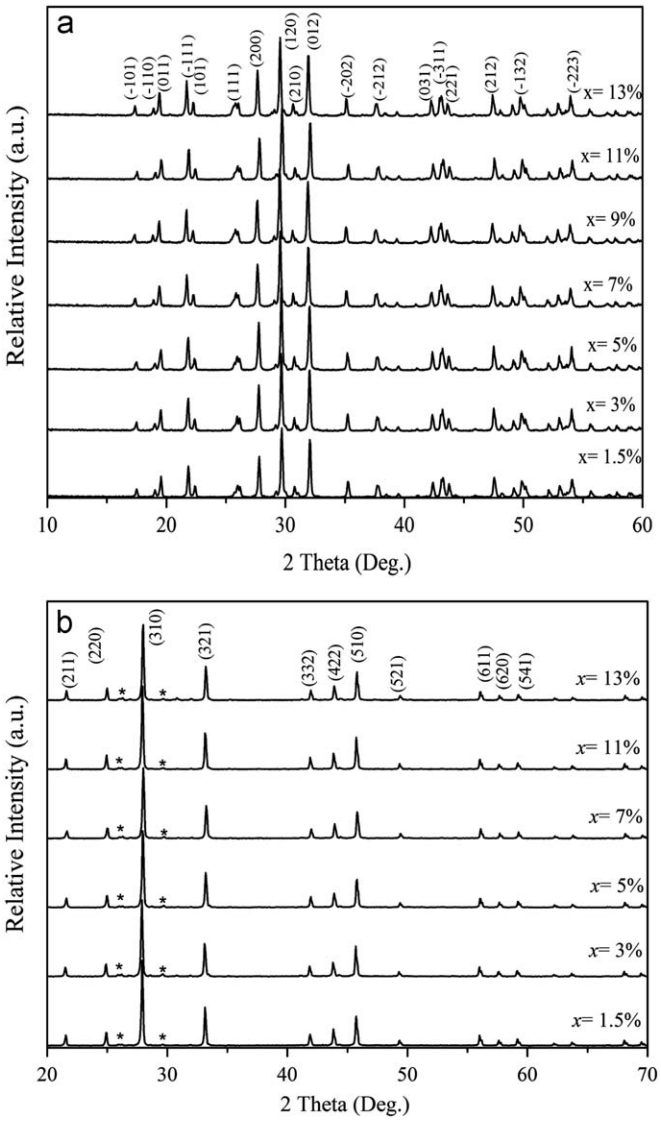

Fig. 1. XRD patterns of $GdPO_4$:xTb^{3+} ($1.5\% \le x \le 13\%$) and $Sr_3Gd(PO_4)_3$:xTb^{3+} ($1.5\% \le x \le 13\%$).

To determine whether quantum cutting occurs in $GdPO_4$:xTb^{3+} ($1.5\% \le x \le 13\%$), the emission spectra of $GdPO_4$:xTb^{3+} ($1.5\% \le x \le 13\%$) excited at 273, 210 and 157 nm were measured (see Fig. 3(a), (b) and (d)). Here, because the peak at 204 nm is near to the ^6G_J–$^8S_{7/2}$ transition of Gd^{3+}, we used 210 nm rather than 204 nm as the excitation wavelength to ensure that the excitation is from the $4f^8$–$4f^7 5d^1$ transition of Tb^{3+}. Moreover, if the origin of the peak at 196 nm differs from that at 210 nm, a different trend in the dependence of the cross relaxation efficiency on the concentration of Tb^{3+} is expected. To further examine the ascription of the peak at 196 nm, we also measured the emission spectra of $GdPO_4$:xTb^{3+} ($1.5\% \le x \le 13\%$) excited at 196 nm. The results are shown in Fig. 3(c). The trends in the luminescence variation are almost the same for all the excitations. The $^5D_3$ emission decreased while the $^5D_4$ emission of Tb^{3+} increased with an increase in the Tb^{3+} content, which is due to the cross relaxation between the $^5D_3 \rightarrow {}^5D_4$ transition and $^7F_6 \rightarrow {}^7F_0$ transitions of Tb^{3+} [26]. Meanwhile, the $^5D_4$ emission reached a maximum at $x = 11\%$ and then decreased, which is caused by concentration quenching effect. The $^5D_4$ emission of Tb^{3+}

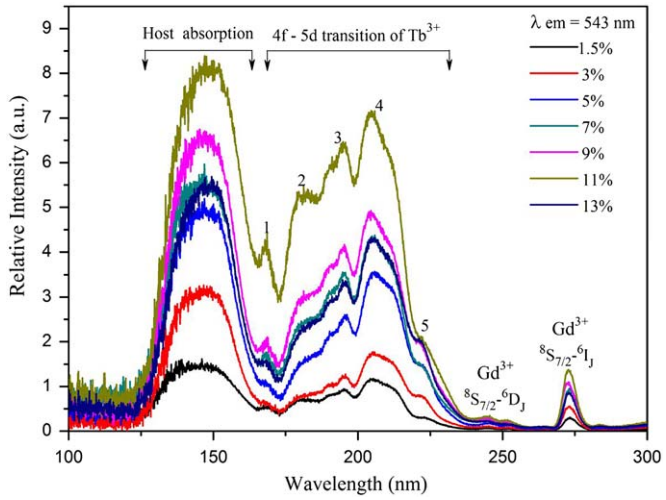

Fig. 2. Excitation spectra of $GdPO_4$:xTb^{3+} ($1.5\% \le x \le 13\%$) monitored by the emission of Tb^{3+} at 543 nm.

increased rapidly with an increase in the concentration of Tb^{3+}. This is due to several factors, including the cross relaxation between the $^5D_3$ and $^5D_4$ levels mentioned above, an increase in the number of luminescence centers, and the quantum cutting, which is discussed in the following section.

3.3. Quantum cutting in $GdPO_4$: Tb^{3+}

As a reference, Fig. 4 depicts the emission spectra of $GdPO_4$:Tb^{3+}(3%) for excitations of 273, 210, 196 and 157 nm. All emission spectra are scaled on the emission intensity for the $^5D_3 \rightarrow {}^7F_6$ transition of Tb^{3+}. By comparing the emission spectra excited at the ^6I_J level of Gd^{3+} (273 nm) with that excited at the other three wavelengths (210, 196 and 157 nm), we find that the percentage of emission from $^5D_4$ is higher than that excited by 273 nm radiation, indicating that quantum cutting occurs in $GdPO_4$:Tb^{3+} (3%). No quantum cutting occurs in $GdPO_4$:Tb^{3+} with excitation of the ^6I_J level of Gd^{3+} (273 nm). When Tb^{3+} ions are excited to their $4f^7 5d^1$ states, the quantum cutting can be explained by a two-step process: cross relaxation and directed energy transfer [3,4] (see Fig. 5(b)). Upon excitation at 210 nm, one Tb^{3+} ion in $GdPO_4$:Tb^{3+} is excited from ground state to its

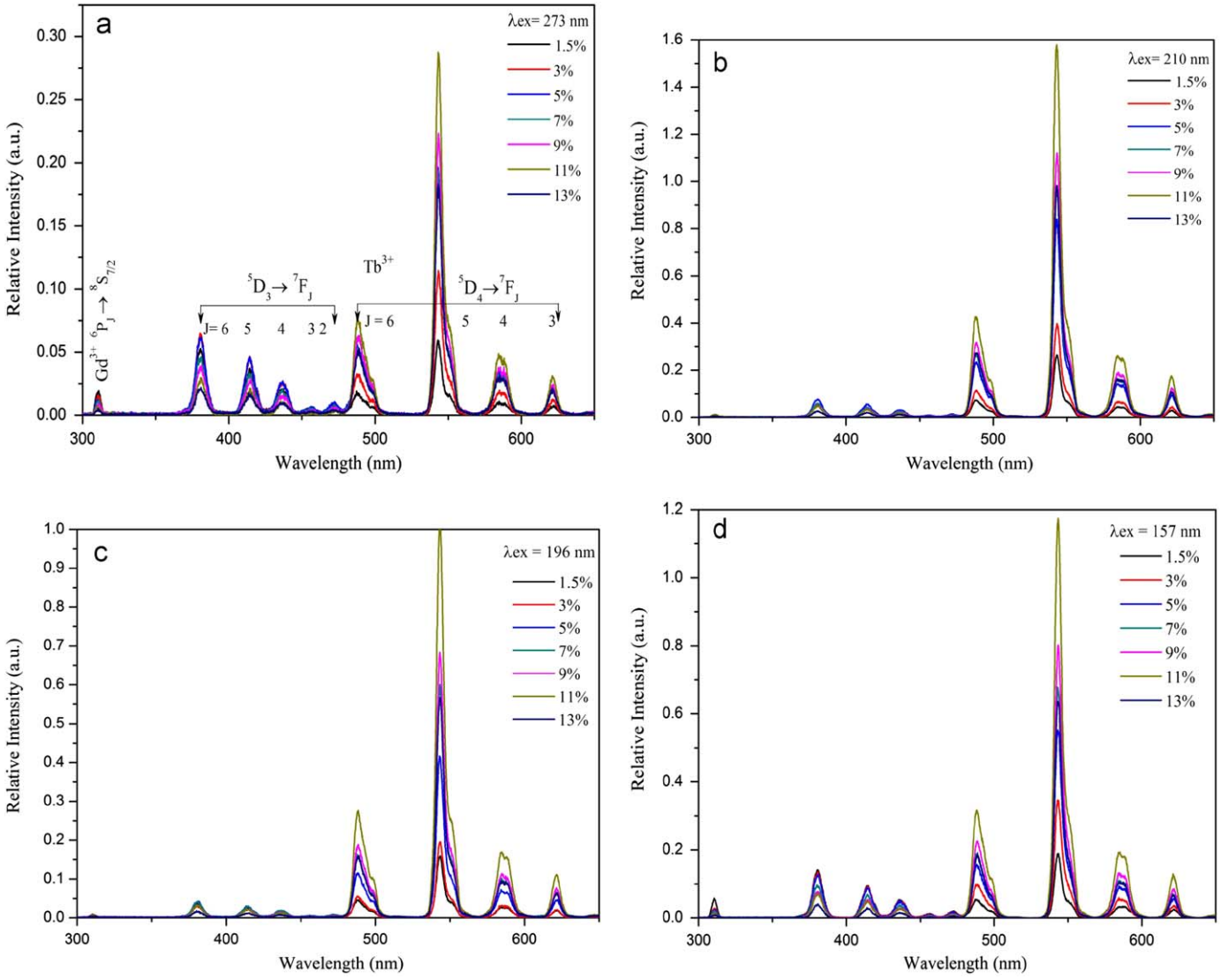

Fig. 3. Emission spectra of $GdPO_4$:xTb^{3+} ($1.5\% \le x \le 13\%$) excited at (a) 273, (b) 210, (c) 196 and (d) 157 nm.

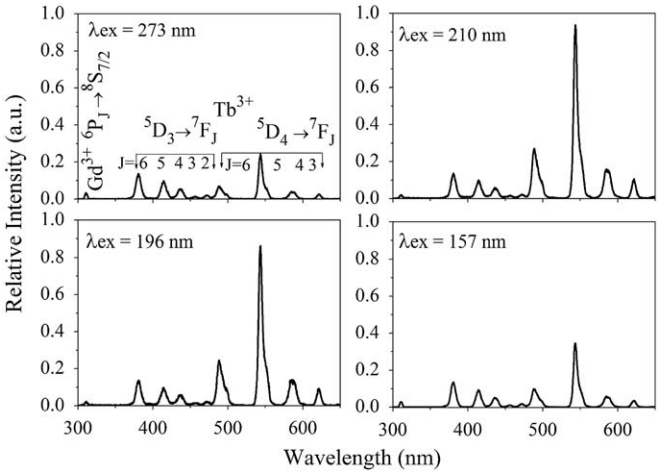

Fig. 4. Emission spectra of $GdPO_4$:Tb^{3+} (3%) under excitations at 273, 210, 196 and 157 nm. All spectra are scaled on the emission intensity for the $^5D_3 \rightarrow {}^7F_6$ transition of Tb^{3+}.

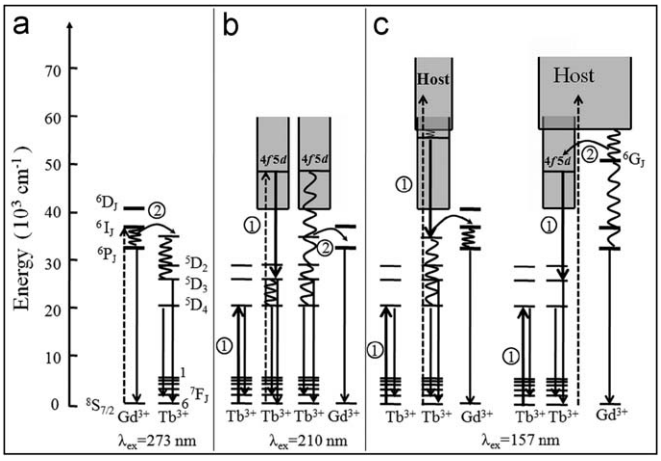

Fig. 5. Energy level diagrams for $GdPO_4$:Tb^{3+} showing the mechanism for visible quantum cutting and the energy transfer process excited at (a) 273, (b) 210 and (c) 157 nm. ① represents cross relaxation and ② represents direct energy transfer.

$4f^75d^1$ state, and subsequently relaxes from the $4f^75d^1$ state to an intermediate state, $^5D_3$. The energy released during the relaxation process is transferred to a neighboring Tb^{3+} ion by cross relaxation, exciting the neighboring Tb^{3+} ion to its $^5D_4$ level, resulting in the first green emission due to the $^5D_4 \rightarrow {}^7F_J$ transition (step 1). The transition from $^5D_3$ state of the original Tb^{3+} generates a second photon (step 2). It is also possible that while Tb^{3+} relaxes from the $4f^75d^1$ state to the $^5D_3$ and $^5D_4$ levels, the released energy is transferred directly to a neighboring Gd^{3+} ion, resulting in the emission observed at 311 nm [3,4]. Taking into account that the emission intensity of Gd^{3+} at 311 nm upon excitation at 157 nm is a little stronger than that upon excitations at 210 and 196 nm (see Fig. 4), and that the host absorption band partially overlaps with the $4f^8$–$4f^75d^1$ transition of Tb^{3+} (see Fig. 2), it is considered that when $GdPO_4$:Tb^{3+} is excited at 157 nm, the energy is first absorbed by host, then is transferred from the host to a higher $4f^75d^1$ state of Tb^{3+}. Subsequently quantum cutting occurs via cross relaxation and direct energy transfer, in a similar way as that observed in $GdPO_4$:Tb^{3+} excited at 210 nm (see Fig. 5(c)). Furthermore, the 157 nm excitation has enough energy to excite Gd^{3+} from its ground state to its ^6G_J state or a much higher state. Because the $4f^8$–$4f^75d^1$ transition of Tb^{3+} in $GdPO_4$ overlaps with the higher excited states of Gd^{3+}, when $GdPO_4$:Tb^{3+} is excited at 157 nm, there may be another energy transfer path (see Fig. 5(c)). Specifically, the excitation energy is first transferred to a higher excited state of Gd^{3+} (such as the ^6G_J state). It is then transferred from Gd^{3+} to the $4f^75d^1$ state of Tb^{3+}, followed by quantum cutting that occurs in a similar way as that observed in $GdPO_4$:Tb^{3+} excited at 210 nm.

The cross relaxation efficiency (η) in this system can be determined by using the following equation, which was first proposed by Wegh et al. [1,15] and later modified by Chen et al. [3,4]:

$$\eta = \frac{P_{CR}}{P_{CR}+P_{DT}} = \frac{R(^5D_4/rest)_{Tb^{3+}} - R(^5D_4/rest)_{Gd^{3+}}}{R(^5D_4/rest)_{Tb^{3+}} + 1} \quad (1)$$

where P_{CR} represents the probability for cross relaxation and P_{DT} is the probability for direct energy transfer. $R(^5D_4/rest)$ is the ratio of the emission intensity of $^5D_4$ to that attributed to $^5D_3$ of Tb^{3+} and ^6P_J of Gd^{3+}. The subscript indicates excitation from Tb^{3+} or Gd^{3+}.

Fig. 6 illustrates the dependence of the calculated cross relaxation efficiency on the concentration (x) of Tb^{3+} in $GdPO_4$:xTb^{3+} ($1.5\% \le x \le 13\%$). The calculated cross relaxation efficiency is fitted by the dotted line. The general trend shows that the cross relaxation efficiency of $GdPO_4$:xTb^{3+} increases from 62% at $x = 1.5\%$ to 75% at $x = 13\%$ under excitation at 210 nm, and increases from 52% at $x = 1.5\%$ to 72% at $x = 13\%$ under excitation at 196 nm. Furthermore, the cross relaxation efficiency of $GdPO_4$:xTb^{3+} increases from 11% at $x = 1.5\%$ to 57% at $x = 13\%$ under excitation at 157 nm. As the concentration of Tb^{3+} increases, the distance between adjacent Tb^{3+} ion decreases. Consequently, the cross relaxation probability between adjacent Tb^{3+} ions increases, resulting in an increase in the cross relaxation efficiency, since the probability of cross relaxation for a dipole–dipole interaction is proportional to L^{-6}, where L is the distance between donor and acceptor ions [27]. The trends of the cross relaxation efficiency of $GdPO_4$:xTb^{3+} ($1.5\% \le x \le 13\%$) excited at 210 and 196 nm are almost the same, indicating that they have almost identical quantum cutting mechanisms, which is an indirect evidence that the peak at 196 nm is mainly due to the $4f^8$–$4f^75d^1$ transition. As discussed above, the energy transfer process of $GdPO_4$:xTb^{3+} excited at 157 nm differs from that excited at 210 and 196 nm. When the energy transfers from the host to a Tb^{3+} or Gd^{3+} ion, part of the energy is lost through nonradiative relaxation, which accounts for why the cross relaxation efficiency

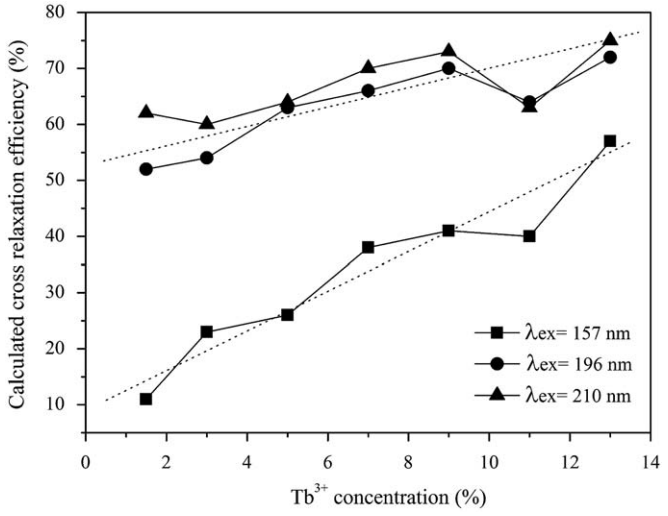

Fig. 6. Dependence of the calculated cross relaxation efficiency on the concentration (x) of Tb^{3+} in $GdPO_4$:xTb^{3+} ($1.5\% \le x \le 13\%$). The trend of the calculated cross relaxation efficiency is fitted with the dotted line.

of $GdPO_4$:xTb^{3+} ($1.5\% \le x \le 13\%$) excited at 157 nm is lower than those for excitations at 210 and 196 nm.

3.4. Photoluminescence properties of $Sr_3Gd(PO_4)_3$:xTb^{3+}

Fig. 7 shows the excitation spectra $Sr_3Gd(PO_4)_3$:xTb^{3+} ($x = 3\%$ and 7%) monitored by the $^5D_4$–$^7F_5$ (543 nm) and $^5D_3$–$^7F_6$ (380 nm) emissions of Tb^{3+}, respectively. The band below 175 nm is assigned to host band absorption [23], while the broad band above 175 nm with a peak at 222 nm is ascribed to the $4f^8$–$4f^75d^1$ transition of Tb^{3+}, which overlaps with the $^8S_{7/2}$–^6G_J transition of Gd^{3+}. The much weaker absorptions at 254 and 273 nm are assigned to the excitation from the $^8S_{7/2}$ ground state to the ^6D_J and ^6I_J states of Gd^{3+}, respectively. Fig. 8 presents the emission spectra of $Sr_3Gd(PO_4)_3$:xTb^{3+}($1.5\% \le x \le 13\%$) excited at 222 and 273 nm. The emission from the $^5D_3$ level decreased with an increase in the Tb^{3+} contents, which is due to the cross relaxation, as mentioned above in regard to $GdPO_4$:Tb^{3+}. But the emission from the $^5D_4$ level, by contrast, did not change much. In particular, when $Sr_3Gd(PO_4)_3$:xTb^{3+} ($1.5\% \le x \le 13\%$) is excited at 273 nm, the emission from the $^5D_4$ level of Tb^{3+} was almost the same. This luminescent behavior is caused by the concentration quenching and quantum cutting effects mentioned in $GdPO_4$:Tb^{3+}. Furthermore, as mentioned in Section 3.1, there are two small unidentified peaks in the XRD patterns of $Sr_3Gd(PO_4)_3$:xTb^{3+}($1.5\% \le x \le 13\%$), which may be caused by a second phase in $Sr_3Gd(PO_4)_3$. The second phase may exist as an impurity which may be also responsible for the luminescent behavior.

3.5. Quantum cutting in $Sr_3Gd(PO_4)_3$:Tb^{3+}

As an example, the emission spectra of $Sr_3Gd(PO_4)_3$:Tb^{3+}(3%) excited at 185, 222 and 273 nm are given in Fig. 9. The spectra are scaled on the $^5D_3 \rightarrow {}^7F_6$ emission. The ratios of $^5D_4$ emission for 185 and 222 nm excitations are higher than that for 273 nm excitation, indicating that quantum cutting occurs in $Sr_3Gd(PO_4)_3$:Tb^{3+} (3%). The quantum cutting process can be considered the same as that in $GdPO_4$:Tb^{3+}. Fig. 10 shows the dependence of the calculated cross relaxation efficiency on the concentration (x) of Tb^{3+} in $Sr_3Gd(PO_4)_3$:xTb^{3+} ($1.5\% \le x \le 13\%$).

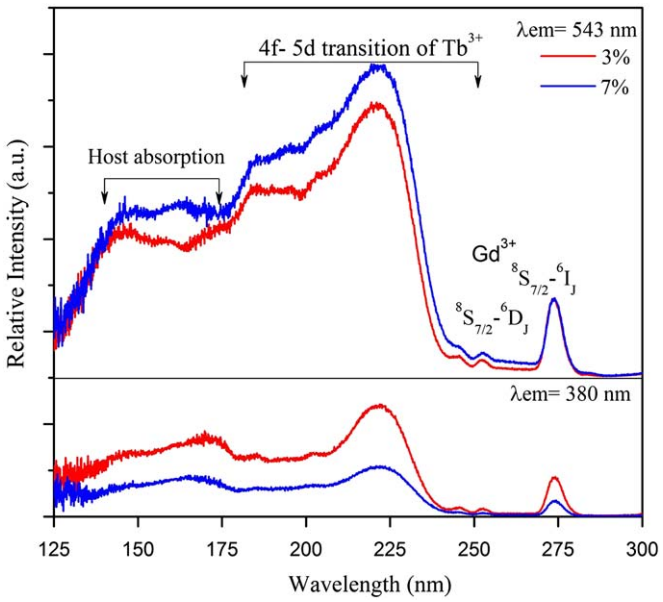

Fig. 7. Excitation spectra of $Sr_3Gd(PO_4)_3$:xTb^{3+} ($x = 3\%$ and 7%) monitored at 543 and 380 nm. Both spectra have the same scales.

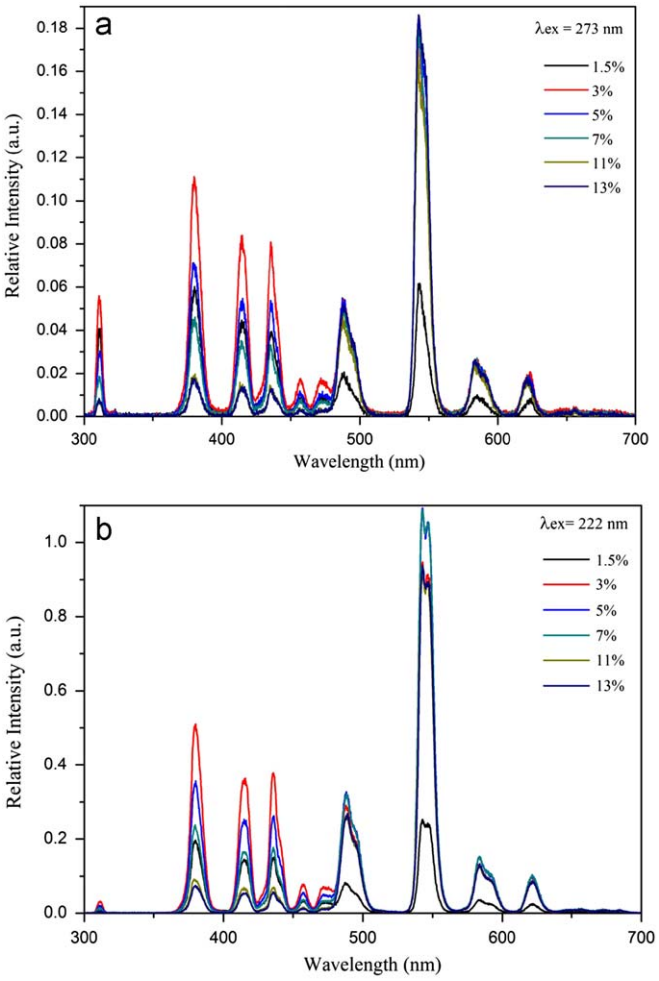

Fig. 8. Emission spectra of $Sr_3Gd(PO_4)_3$:xTb^{3+} ($1.5\% \le x \le 13\%$) excited at (a) 273 nm and (b) 222 nm.

Upon excitation at 222 nm, the calculated cross relaxation efficiency for $Sr_3Gd(PO_4)_3$:xTb^{3+} is 15% for a sample with $x = 1.5\%$ and 21% for sample with $x = 13\%$. Meanwhile, the calculated cross relaxation efficiency for $Sr_3Gd(PO_4)_3$:xTb^{3+} is 13% for a sample with $x = 1.5\%$ and 26% for sample with $x = 13\%$ under excitation at 185 nm. The cross relaxation efficiency variation of $Sr_3Gd(PO_4)_3$:xTb^{3+} ($1.5\% \le x \le 13\%$) showed a slow growing trend. Comparing with $GdPO_4$:xTb^{3+} ($1.5\% \le x \le 13\%$), at the same Tb^{3+} doping concentration, the cross relaxation efficiency of $Sr_3Gd(PO_4)_3$:xTb^{3+} ($1.5\% \le x \le 13\%$) is rather low. This is partly due to the differences of Gd^{3+}–Gd^{3+} distances in these crystals, according to the theory that the probability of cross relaxation is inversely proportional to L^6. The nearest-neighboring Gd^{3+}–Gd^{3+} distance (4.03 Å) in $Sr_3Gd(PO_4)_3$ is longer than that (3.41 Å) in $GdPO_4$, as estimated based on atomic coordinates in $Sr_3La(PO_4)_3$ [25] and $GdPO_4$ [24], and lattice constants determined by X-ray diffraction. Therefore, the probability of cross relaxation is lower in $Sr_3Gd(PO_4)_3$:Tb^{3+} than in $GdPO_4$:Tb^{3+}. In addition, the lower cross relaxation efficiency in $Sr_3Gd(PO_4)_3$:xTb^{3+} may also be due to a high concentration of defects or impurities in them.

4. Conclusions

By utilizing Tb^{3+}–Tb^{3+} pairs, quantum cutting has been realized in two kinds of oxide hosts.

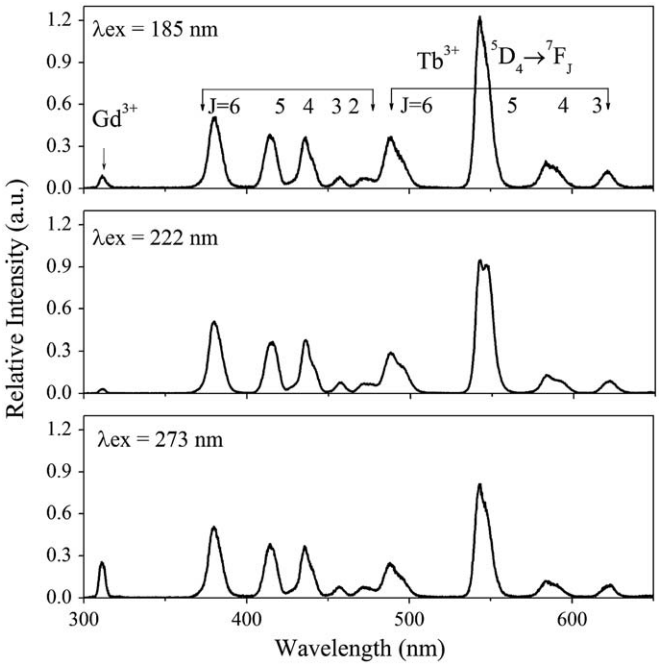

Fig. 9. Emission spectra of $Sr_3Gd(PO_4)_3$:Tb^{3+} (3%) upon excitations at (a) 273, (b) 221 and (c) 185 nm. The spectra are scaled on the $^5D_3 \rightarrow {}^7F_6$ transition of Tb^{3+}.

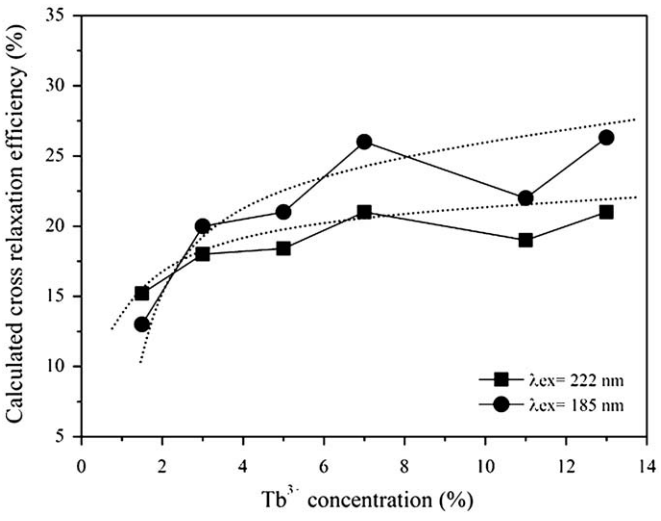

Fig. 10. Dependence of the calculated cross relaxation efficiency on the concentration (x) of Tb^{3+} in $Sr_3Gd(PO_4)_3$:xTb^{3+} ($1.5\% \leq x \leq 13\%$). The trend of the calculated cross relaxation efficiency variation is fitted with the dotted line.

Upon excitation in the $4f^75d^1$ states of Tb^{3+} in $GdPO_4$:Tb^{3+} and $Sr_3Gd(PO_4)_3$:Tb^{3+}, the excitation energy is transferred via a quantum cutting process: the Tb^{3+} ion first relaxes from the $4f^75d^1$state to an intermediate ^5D_J state. During the relaxation, the released energy excites a neighboring Tb^{3+} to its $^5D_4$ level by cross relaxation and/or transfers directly to a neighboring Gd^{3+}, depending on the excitation wavelength. Then, the original Tb^{3+} and the neighboring Tb^{3+} and/or Gd^{3+} ions revert to their ground states by emitting two photons.

When $GdPO_4$:Tb^{3+} is excited at the host absorption (157 nm), the excitation energy is first absorbed by host, then is transferred through two paths: (a) the absorbed energy is transferred to the $4f5d$ state of a Tb^{3+}, then relaxes via a quantum cutting process, or (b) the absorbed energy is transferred to a higher $4f$ state of Gd^{3+}(e.g. ^6G_J), then is transferred to the $4f5d$ state of a Tb^{3+}, subsequently relaxes via a quantum cutting process.

An increase in the Tb^{3+} content increases the cross relaxation probability between two neighboring Tb^{3+} ions in $GdPO_4$:xTb^{3+} and $Sr_3Gd(PO_4)_3$:xTb^{3+}; as a result, the cross relaxation efficiency for $GdPO_4$:xTb^{3+} and $Sr_3Gd(PO_4)_3$:xTb^{3+} is increased. When Tb^{3+} content in $GdPO_4$:xTb^{3+} increases from $x = 1.5\%$ to 13%, the cross relaxation efficiency of $GdPO_4$:xTb^{3+} increases from 62% to 75% under excitation at 210 nm and from 11% to 57% under excitation at 157 nm.

Acknowledgments

This work was in part supported by a Grant-in-Aid for Exploratory Research from the Japan Society for the Promotion of Science (Grant no. 19656164). One of the authors (Dr. Wang) gratefully acknowledges Y.H. Wang for helpful discussion and the China Scholarship Council (CSC) for financial support.

References

[1] R.T. Wegh, H. Donker, K.D. Oskam, A. Meijerink, Science 283 (1999) 663–666.
[2] Y. Zhou, S.P. Felfilov, H.J. Seo, J.Y. Jeoug, D.A. Keszler, R.S. Meltzer, Phys. Rev. B 77 (2008) 075129–075134.
[3] T.J. Lee, L.Y. Luo, E.W.G. Diau, T.M. Chen, Appl. Phys. Lett. 89 (2006) 131121–131123.
[4] H.Y. Tzeng, B.M. Cheng, T.M. Chen, J. Lumin. 122–123 (2007) 917–920.
[5] W.W. Piper, J.A. de Luca, F.S. Ham, J. Lumin. 8 (1974) 344–348.
[6] F.T. You, S.H. Huang, C.X. Meng, G.B. Zhang, J. Lumin. 122–123 (2007) 58–61.
[7] F.B. Xiong, Y.F. Lin, Y.J. Chen, Y.D. Huang, Chem. Phys. Lett. 429 (2006) 410–414.
[8] R.T. Wegh, H. Donker, A. Meijerink, J. Holsa, Phys. Rev. B 56 (1997) 13841–13848.
[9] Z. Yang, H.H. Lin, M.Z. Su, W. Wang, J. Alloys Compd. 308 (2000) 94–97.
[10] S.P. Felfilov, Y. Zhou, H.J. Seo, J.Y. Jeoug, D.A. Keszler, R.S. Meltzer, Phys. Rev. B 74 (2006) 085101–085110.
[11] N. Kodama, Y. Watanabe, Appl. Phys. Lett. 84 (2004) 4141–4144.
[12] N. Kodama, S. Oishi, J. Appl. Phys. 98 (2005) 103515–103520.
[13] M. Karbowiak, A. Mech, W. Ryba-Romanowski, J. Lumin. 114 (2005) 65–70.
[14] P. Vergeer, T.J.H. Vlugt, M.H.F. Kox, M.I. den Hertog, J.P.J.M. van der Eerden, A. Meijerink, Phys. Rev. B 71 (2005) 014119–014130.
[15] R.T. Wegh, E.V.D. van Loef, A. Meijerink, J. Lumin. 90 (2000) 111–122.
[16] B. Liu, Y. Chen, C. Shi, Y. Tao, J. Lumin. 101 (2005) 155–159.
[17] T.J. Lee, L.Y. Luo, B.M. Cheng, W.G. Diau, T.M. Chen, Appl. Phys. Lett. 92 (2008) 081106–081109.
[18] Z.F. Tian, H.B. Liang, H.H. Lin, Q. Su, J. Solid State Chem. 179 (2006) 1356–1362.
[19] Y.H. Wang, C.F. Wu, J. Wei, J. Lumin. 126 (2007) 503–507.
[20] K.K. Lee, Y.C. Kang, K.Y. Jung, H.D. Park, Jpn. J. Appl. Phys. Part 1 41 (2002) 5590–5593.
[21] X.Y. Wu, H.P. You, B.Y. Yu, C.H. Park, Mater. Res. Bull. 37 (2002) 1531–1538.
[22] L. Li, G. Li, D. Wang, Y. Tao, X. Zhang, Sci. China Ser. E 49 (2006) 408–413.
[23] H.B. Liang, Y. Tao, J.H. Xu, Q. Su, J. Solid State Chem. 177 (2004) 901–908.
[24] D.F. Mullica, D.A. Grossie, Inorg. Chim. Acta 109 (1985) 105–110.
[25] T. Znamierowska, W. Szuszkiewicz, J. Hanuza, L. Macalik, D. Hreniak, J. Alloys Compd. 341 (2002) 371–375.
[26] G. Blasse, B.C. Grabmaier, Luminescent Materials, Springer, Berlin, 1994, pp. 91–102 (Chapter 5).
[27] B. Henderson, G.F. Imbusch, Optical Spectroscopy of Inorganic Solids, Clarendon Press, Oxford, 1989, pp. 151–197 (Chapter 5).